

Article

# Molecular Engineering of High Energy Barrier in Single-Molecule Magnets Based on $[\text{Mo}^{\text{III}}(\text{CN})_7]^{4-}$ and V(II) Complexes

Vladimir S. Mironov 

Shubnikov Institute of Crystallography of Federal Scientific Research Centre "Crystallography and Photonics" RAS, Leninsky Prospect 59, 119333 Moscow, Russia; mirsa@list.ru; Tel.: +7-905-708-5211

Received: 1 May 2018; Accepted: 28 May 2018; Published: 30 May 2018



**Abstract:** Molecular engineering of high energy barrier  $U_{\text{eff}}$  in single-molecule magnets (SMMs) of general composition  $\text{Mo}^{\text{III}}_k\text{V}^{\text{II}}_m$  based on orbitally-degenerate pentagonal-bipyramidal  $[\text{Mo}^{\text{III}}(\text{CN})_7]^{4-}$  complexes with unquenched orbital momentum and high-spin V(II) complexes is discussed. In these SMMs, the barrier originates exclusively from anisotropic Ising-type exchange interactions  $-J_{xy}(S_i^x S_j^x + S_i^y S_j^y) - J_z S_i^z S_j^z$  in the apical cyano-bridged pairs  $\text{Mo}^{\text{III}}\text{-CN-V}^{\text{II}}$ , which produce a double-well energy profile with a doubly degenerate ground spin state  $\pm M_S$ . It is shown that the spin-reversal barrier  $U_{\text{eff}}$  is controlled by anisotropic exchange parameters  $J_z, J_{xy}$ , and the number  $n$  of apical  $\text{Mo}^{\text{III}}\text{-CN-V}^{\text{II}}$  groups in a SMM cluster,  $U_{\text{eff}} \sim 0.5 |J_z - J_{xy}| n$ ; it can reach a value of many hundreds of wavenumbers (up to  $741 \text{ cm}^{-1}$ ). This finding provides a very efficient straightforward strategy for further scaling  $U_{\text{eff}}$  to high values ( $>1000 \text{ cm}^{-1}$ ) by means of enhancing exchange parameters  $J_z, J_{xy}$ , and increasing the number of  $[\text{Mo}^{\text{III}}(\text{CN})_7]^{4-}$  complexes in a SMM molecule.

**Keywords:** single-molecule magnet; magnetic anisotropy; spin-reversal barrier; anisotropic exchange interactions; Molybdenum(III) heptacyanometallate

## 1. Introduction

Single-molecule magnets (SMMs) are individual high-spin molecules featuring slow spin relaxation and preserving their magnetic moment below characteristic blocking temperature  $T_B$  [1–7]. The slow relaxation of SMMs is caused by a double-well potential with the two lowest  $M_S = +S$  and  $M_S = -S$  spin states separated by an energy barrier  $U_{\text{eff}}$ , which arises from the combined effect of the easy-axis (Ising-type) magnetic anisotropy (quantified by the axial zero-field splitting parameter  $D$ ) and high-spin ground state  $S$ . The spin-reversal barrier  $U_{\text{eff}}$  is expressed by  $|D|S^2$  or  $|D|(S^2 - 1/4)$  for integer and half-integer spins, respectively. Since the discovery of the first representative ( $\text{Mn}_{12}\text{Ac}$ ) in 1993 [1,2], SMMs have attracted increasing attention due to their huge forward-looking application potential in the design of high-density information storage [8], quantum computing [9–12], and molecular spintronics [13,14]. Currently, development of SMMs is one of the most rapidly growing lines of research in the field of molecular magnetism. However, rapid advance of the SMM-based technology is hampered by a low blocking temperature  $T_B$ , which is normally below a few Kelvins [1–7]. Designing of SMMs with higher  $T_B$  and  $U_{\text{eff}}$  characteristics has remained a highly challenging task over the past two decades. Earlier efforts toward increasing  $U_{\text{eff}}$  and  $T_B$  were mainly focused on obtaining large polynuclear transition metal complexes (mostly based on  $\text{Mn}^{\text{III}}$  ions) with a high ground-state spin  $S$ . However, as these studies progressed, it was realized that the barrier  $U_{\text{eff}}$  and temperature  $T_B$  do not generally rise with increasing spin and nuclearity of a magnetic molecule because the overall magnetic anisotropy  $D$  is inversely proportional to the square of the spin,  $D \sim S^{-2}$  [15–17].

In fact, the barrier  $U_{\text{eff}} = |D|S^2$  is largely independent on spin  $S$ ; consequently, the barrier  $U_{\text{eff}}$  can be increased only by increasing the molecular magnetic anisotropy  $D$ . Basically, magnetic anisotropy  $D$  originates from a combined effect of spin-orbit coupling and some orbital angular momentum; it may operate as a first-order perturbation or as a second-order perturbation, depending on the nature of the ground state. In SMMs based on high-spin 3d ions, magnetic anisotropy  $D$  originates from single-ion contributions resulting from zero field splitting (ZFS) on individual magnetic ions. Being the product of a second-order effect, the ZFS energy is relatively small, typically within few tens of  $\text{cm}^{-1}$  or less for spin-only 3d-ions (such as  $\text{Mn}^{\text{III}}$ ,  $\text{Fe}^{\text{III}}$ , and  $\text{Ni}^{\text{II}}$ ); thus, it leads generally to a rather small magnetic anisotropy  $D$  and low barriers  $U_{\text{eff}}$  [15–17]. Much stronger first-order magnetic anisotropy is produced by magnetic ions with the unquenched orbital momentum, such as lanthanide and actinide ions [18–21]. Indeed, all lanthanide ions with open 4f-shell (except  $\text{Gd}^{3+}$ ) exhibit large unquenched orbital momentum, which, in concert with strong spin-orbit coupling and weak crystal-field splitting of 4f states, produces extremely strong single-ion magnetic anisotropy of  $\text{Ln}^{3+}$  ions; these features taken together ultimately lead to high  $U_{\text{eff}}$  and  $T_{\text{B}}$  values of Ln-based SMMs. With the discovery of the first Ln-based SMM, the double decker mononuclear complex  $[(\text{Pc})_2\text{Tb}]^-$  ( $\text{Pc}$  = phthalocyanine) in 2003 [22], lanthanide complexes have opened a new avenue to high-performance SMMs [23–28]. Even mononuclear lanthanide complexes exhibit slow magnetic relaxation at low temperatures with a high barrier  $U_{\text{eff}}$ ; they are referred to as single-ion magnets (SIMs) [18–29]. The last few years have seen impressive progress in designing advanced SIMs with new record blocking temperature, such as  $T_{\text{B}} = 20$  K [30], and spin-reversal barrier  $U_{\text{eff}} = 1261$   $\text{cm}^{-1}$  (1815 K) [31]. Recently, new record SMM characteristics were reported for a mononuclear dysprosium complex  $[\text{Dy}(\text{Cp}(\text{t-Bu}_3)_2)^+]$ ,  $U_{\text{eff}}/k_{\text{B}} = 1760$  K,  $T_{\text{B}} = 60$  K [32,33]. These values are an order of magnitude higher than those known for SMMs based on polynuclear transition metal complexes,  $U_{\text{eff}} = 62$   $\text{cm}^{-1}$  and  $T_{\text{B}} = 4.5$  K for a  $\text{Mn}_6$  complex with  $S = 12$  [34].

More recently, there has also been a growing interest in mononuclear 3d complexes with unquenched first-order orbital momentum, which is provided by a special less-common coordination of the metal atom. Especially interesting are complexes with a large uniaxial magnetic anisotropy (Ising spin units), which are capable to behave as SIMs with a large energy barrier originating from the first-order spin-orbit splitting of the orbitally degenerate ground state [35–38]. In recent years, there have been numerous reports on monometallic 3d complexes with SIM behavior [35,36]. Among them, the largest  $U_{\text{eff}}$  barrier has been obtained for linear two-coordinated Fe(I) [37] and Co(II) [38] complexes (246 and 413  $\text{cm}^{-1}$ , respectively); high energy barriers were also reported for other low-coordinated 3d transition metal complexes [39–42].

These results vividly show that magnetic centers with unquenched orbital angular momentum provide great opportunities to maximize magnetic anisotropy and to achieve a high barrier and blocking temperature. However, it should be emphasized that the current record-breaking SMM characteristics are based exclusively on single-center magnetic anisotropy of high-spin monometallic complexes, which is already close to the physical limits for 4f and 3d ions. In fact, the maximum feasible barrier  $U_{\text{eff}}$  in 4f-SIMs is specified by the total crystal-field splitting energy of the ground  $J$ -multiplet of  $\text{Ln}^{3+}$  ions, which is normally within several hundreds of  $\text{cm}^{-1}$  and very rarely reaches 1000  $\text{cm}^{-1}$  or higher [43]. Therefore, the current record barrier around 1250  $\text{cm}^{-1}$  for Dy-based SIMs [32,33] is close to the maximum CF splitting energy for lanthanide ions and thus it is difficult to increase the barrier far beyond this value [44]. The same is also true for mononuclear high-spin 3d complexes with unquenched orbital momentum, in which maximum value of  $U_{\text{eff}}$  is controlled by the spin-orbit splitting energy of the ground orbital manifold; this energy is limited by ca. 1000  $\text{cm}^{-1}$  due to weak spin-orbit coupling for 3d electrons.

Alternative strategy toward high-performance SMMs is based on pair-ion contributions to the molecular magnetic anisotropy  $D$  rather than on single-ion contributions [45]. These pair-ion contributions are associated with anisotropic exchange interactions produced by low-spin ( $S = 1/2$ ) orbitally-degenerate 4d and 5d complexes with unquenched orbital angular momentum, such as

pentagonal-bipyramidal (PBP) complexes  $[\text{Mo}^{\text{III}}(\text{CN})_7]^{4-}$  [45–47] and  $[\text{Re}^{\text{IV}}(\text{CN})_7]^{3-}$  [46,48,49], and octahedral hexacyano complexes  $[\text{Ru}^{\text{III}}(\text{CN})_6]^{3-}$  [50] and  $[\text{Os}^{\text{III}}(\text{CN})_6]^{3-}$  [51]. It is noteworthy that, unlike high-spin 4f and 3d complexes, these complexes exhibit no single-ion magnetic anisotropy in the usual sense, i.e., as the ZFS of the ground-state spin multiplet  $2S + 1$  (which occurs at  $S > 1/2$ ). Instead, their single-ion magnetic anisotropy can be seen only in an anisotropic  $g$ -tensor and in anisotropic magnetic susceptibility; moreover, it can completely disappear for magnetically isotropic  $[\text{Ru}^{\text{III}}(\text{CN})_6]^{3-}$  and  $[\text{Os}^{\text{III}}(\text{CN})_6]^{3-}$  octahedral complexes [50,51]. In this case, the unquenched orbital momentum of low-spin orbitally degenerate 4d and 5d complexes affects the overall magnetic anisotropy through highly anisotropic exchange interactions with other spin carriers [45–47,49]. Thus, being incorporated into polynuclear heterometallic spin clusters together with high-spin 3d ions, these 4d/5d complexes form pair-ion 4d/5d–3d anisotropic exchange interactions, which can produce high magnetic anisotropy  $D$  and spin reversal barrier  $U_{\text{eff}}$  [45–47,49]. It is important to note, however, that the anisotropic exchange interactions in themselves do not necessarily lead to a SMM behavior because of the condition for a molecular spin cluster to have a negative magnetic anisotropy with a small transverse component ( $D < 0$ ,  $E \sim 0$ ) [52,53]. For this, two additional conditions are needed: (i) the anisotropic exchange interactions must have the Ising-type character,  $-J_{xy}(S_i^x S_j^x + S_i^y S_j^y) - J_z S_i^z S_j^z$  with  $|J_z| \gg |J_{xy}|$ ; and (ii) the anisotropic exchange parameters  $J_z, J_{xy}$  must be large in absolute value. Actually, among known orbitally-degenerate complexes, only PBP complexes  $[\text{Mo}^{\text{III}}(\text{CN})_7]^{4-}$  and  $[\text{Re}^{\text{IV}}(\text{CN})_7]^{3-}$  fully meet these conditions [45–54]. As shown in our previous works, these complexes have a unique property to form uniaxial anisotropic spin coupling  $H_{\text{eff}} = -J_{xy}(S_{\text{M}}^x S_{\text{Mn}}^x + S_{\text{M}}^y S_{\text{Mn}}^y) - J_z S_{\text{M}}^z S_{\text{Mn}}^z$  ( $\text{M} = \text{Mo}^{\text{III}}, \text{Re}^{\text{IV}}$ ) with high-spin  $\text{Mn}^{\text{II}}$  ions ( $S = 5/2$ ) attached in both the apical and equatorial coordination positions; remarkably, the uniaxial symmetry of the spin Hamiltonian  $H_{\text{eff}}$  retains even for the actual low symmetry M–CN–Mn exchange-coupled pairs [47,49]. The apical pairs M–CN–Mn exhibit Ising-type anisotropic exchange interactions ( $|J_z| > |J_{xy}|$ ), while exchange interaction in the equatorial pairs is nearly isotropic with a small easy-axis ( $xy$ ) anisotropic component ( $|J_z| < |J_{xy}|$ ,  $|J_z - J_{xy}| \ll |J_z|$ ) [47,49]. Ising-type exchange interactions of apical pairs are especially important since they generate uniaxial magnetic anisotropy of the necessary quality (i.e.,  $D < 0$ ,  $E \sim 0$ ) and form a barrier. Thus, in the  $\text{Mo}^{\text{III}}\text{Mn}^{\text{II}}_2$  trinuclear complex composed of central  $[\text{Mo}^{\text{III}}(\text{CN})_7]^{4-}$  complex and two  $\text{Mn}^{\text{II}}$  ions in the apical positions, Ising-type exchange interactions  $-J_{xy}(S_{\text{Mo}}^x S_{\text{Mn}}^x + S_{\text{Mo}}^y S_{\text{Mn}}^y) - J_z S_{\text{Mo}}^z S_{\text{Mn}}^z$  of two apical  $\text{Mo}^{\text{III}}\text{–CN–Mn}^{\text{II}}$  pairs (with  $J_z = -34$ ,  $J_{xy} = -11 \text{ cm}^{-1}$ ) form a double-well potential with the energy barrier of  $40.5 \text{ cm}^{-1}$  (58.5 K) and blocking temperature  $T_{\text{B}} = 3.2 \text{ K}$  [55]. Quite recently, another related  $\text{Mo}^{\text{III}}\text{Mn}^{\text{II}}_2$  SMM complex with very close characteristics ( $U_{\text{eff}} = 44.9 \text{ cm}^{-1}$ ,  $T_{\text{B}} = 2.5 \text{ K}$ ,  $J_z = -35.4$ ,  $J_{xy} = -11.4 \text{ cm}^{-1}$ ) was reported [56]. Remarkably, in these systems, the barrier  $U_{\text{eff}}$  is controlled exclusively by the anisotropic exchange parameters (namely, by the difference  $|J_z - J_{xy}|$ ) and by the number  $n$  of the apical exchange-coupled pairs  $\text{Mo}^{\text{III}}\text{–CN–Mn}^{\text{II}}$ ,  $U_{\text{eff}} \approx |J_z - J_{xy}| n$  [47] (Figure 1).

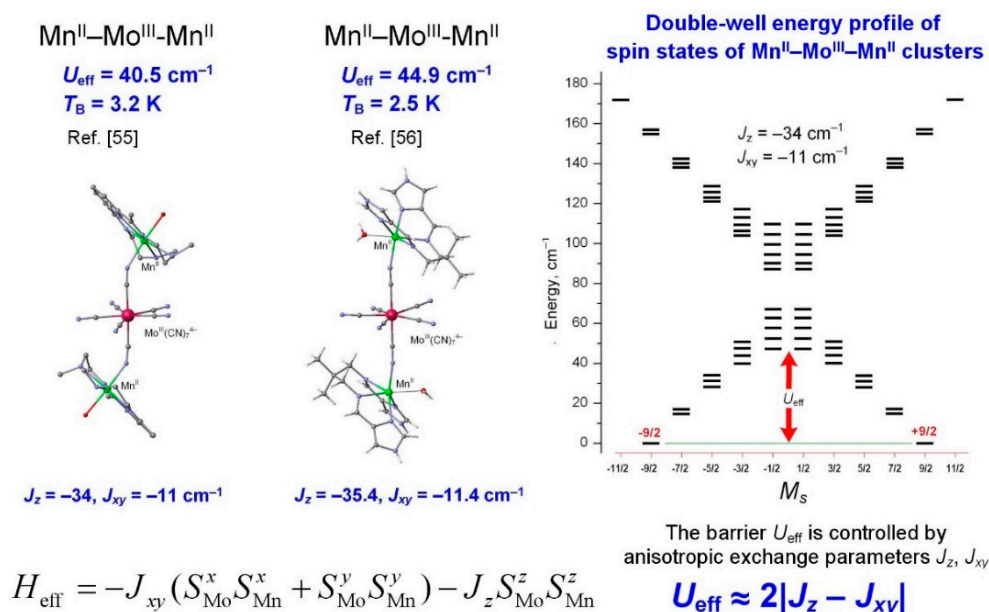


**Figure 1.** Origin of SMM behavior of Mn<sup>II</sup>-Mo<sup>III</sup>-Mn<sup>II</sup> clusters [55,56]. Anisotropic exchange interactions in two apical groups Mo-CN-Mn are described by the uniaxial spin Hamiltonian  $H_{\text{eff}} = -J_{xy}(S_i^x S_j^x + S_i^y S_j^y) - J_z S_i^z S_j^z$  of the Ising type ( $|J_z| > |J_{xy}|$ ), which result in a double-well energy profile with the ground doubly degenerate quantum spin states  $M_S = +9/2$  and  $M_S = -9/2$  separated by the energy barrier  $U_{\text{eff}}$ . The latter is controlled by the anisotropic exchange parameters,  $U_{\text{eff}} \approx 2|J_z - J_{xy}|$  [47].

This opens new avenues for a significant increase in the barrier and the blocking temperature both by enhancing exchange interactions and by increasing nuclearity of the SMM cluster [45–47]. To further develop this strategy, this article develops theoretical frameworks for obtaining high SMM characteristics in some hypothetical 4d–3d heterometallic polynuclear complexes based on [Mo<sup>III</sup>(CN)<sub>7</sub>]<sup>4−</sup> heptacyanometallate and V<sup>II</sup> ions. In these systems, high  $U_{\text{eff}}$  and  $T_{\text{B}}$  values could potentially be obtained due to much stronger exchange interactions in Mo<sup>III</sup>-CN-V<sup>II</sup> cyano-bridged pairs, i.e.,  $J > 200 \text{ cm}^{-1}$  for V<sup>II</sup> [57–59] vs.  $J \sim 40 \text{ cm}^{-1}$  for Mn<sup>II</sup> [55,56]. It is important to emphasize that this system fully meets the specific requirements for orbitally-degenerate complexes, which are necessary for obtaining a high barrier. In this respect, it is relevant to note that anisotropic exchange interactions were also observed in other heterometallic cyano-bridged transition-metal complexes [53,54]; among 3d-based cyano-bridged complexes, anisotropic exchange was first reported in a {LCu<sup>II</sup>-NC-Fe<sup>III</sup>(CN)<sub>5</sub>} ferromagnetically coupled cluster [60]. However, as is shown below, most of the d-complexes featuring anisotropic exchange are of little interest in increasing SMM characteristics, either due to small exchange parameters or because of low symmetry of the anisotropic spin Hamiltonian. As for lanthanide-based SMMs, 4f-3d anisotropic exchange contributions to the  $U_{\text{eff}}$  barrier and hysteresis have recently been shown to be important in heterometallic {Cr<sup>III</sup><sub>2</sub>Dy<sup>III</sup><sub>2</sub>} SMM clusters [61,62]. At the same time, it is clear that lanthanide ions are generally not good candidates for the efficient implementation of the claimed strategy owing to inherently weak exchange interactions resulting from the core-like nature of 4f electrons.

The aim of this work is to establish main regularities in the variation of the spin-reversal barrier  $U_{\text{eff}}$  in heterometallic Mo<sup>III</sup>-V<sup>II</sup> molecular spin clusters, depending on their size, composition and topology of anisotropic and isotropic exchange linkages. It is of special interest to explore the interplay between anisotropic exchange interactions in the apical Mo<sup>III</sup>-CN-V<sup>II</sup> pairs and isotropic exchange interactions in the equatorial pairs and to analyze their impact on the overall magnetic anisotropy and barrier. Some specific approaches to engineering high energy barrier in terms of anisotropic exchange interactions are discussed.

## 2. Results and Discussion

### 2.1. Electronic Structure of $[\text{Mo}^{\text{III}}(\text{CN})_7]^{4-}$ Complex

This section discusses the basic mechanism of anisotropic exchange interactions between  $[\text{Mo}^{\text{III}}(\text{CN})_7]^{4-}$  complexes and  $\text{V}^{\text{II}}$  ions. In fact, this mechanism is similar to that considered earlier for the spin coupling between  $[\text{Mo}^{\text{III}}(\text{CN})_7]^{4-}$  and  $\text{Mn}^{\text{II}}$  [47] complexes, since in both cases strong exchange anisotropy in the  $\text{Mo}^{\text{III}}\text{-CN-M}(3d)$  pairs is caused by the unquenched angular orbital angular momentum of the PBP complex  $[\text{Mo}^{\text{III}}(\text{CN})_7]^{4-}$ . Although the electronic structure and magnetic properties of  $[\text{Mo}^{\text{III}}(\text{CN})_7]^{4-}$  were previously discussed in detail in Ref. [45,47], it is still appropriate to provide here an overview of its main characteristics, which are essential for understanding specific details of the origin of strong exchange anisotropy. In the PBP ligand surrounding, the two lowest degenerate orbitals  $4d_{xz}$  and  $4d_{yz}$  are populated by three electrons to produce an orbital doublet  ${}^2\Phi_{xz,yz} = {}^2\Phi(M_L = \pm 1)$ , whose two components correspond to the  $M_L = \pm 1$  projection of the unquenched angular orbital momentum  $L$  on the polar  $z$ -axis of the  $[\text{Mo}(\text{CN})_7]^{4-}$  bipyramid. The  ${}^2\Phi(M_L = \pm 1)$  wave functions are represented by two degenerate electronic configurations  $(d_{+1})^2(d_{-1})^1$  and  $(d_{-1})^2(d_{+1})^1$  with  $d_{\pm 1} = (d_{xz} \pm id_{yz})/\sqrt{2}$  being complex  $d$  orbitals with definite projection of the orbital momentum ( $m_l = \pm 1$ ) on the polar axis of the pentagonal bipyramid (Figure 2). Alternatively, the real wave functions are expressed by  ${}^2\Phi_{xz} = (d_{yz})^2(d_{xz})^1$  and  ${}^2\Phi_{yz} = (d_{xz})^2(d_{yz})^1$ . The orbital doublet  ${}^2\Phi$  undergoes spin-orbit splitting ( $\zeta_{\text{Mo}}LS$ ) into the ground  $\varphi(\pm 1/2)$  and excited  $\chi(\pm 1/2)$  Kramers doublets (Figure 2). In the strong pentagonal-bipyramidal ligand field, the  $\varphi(\pm 1/2)$  wave functions are well described by the single-determinant electronic configurations  $(d_{+1})^2(d_{-1})\uparrow$  and  $(d_{-1})^2(d_{+1})\downarrow$  with unquenched orbital momentum ( $L_z = \pm 1$ , Figure 2) [45,47]. As a result,  $[\text{Mo}(\text{CN})_7]^{4-}$  complex exhibits highly anisotropic  $g$ -tensor (such as  $g_z = 3.89$  and  $g_x = g_y = 1.77$  [63]).

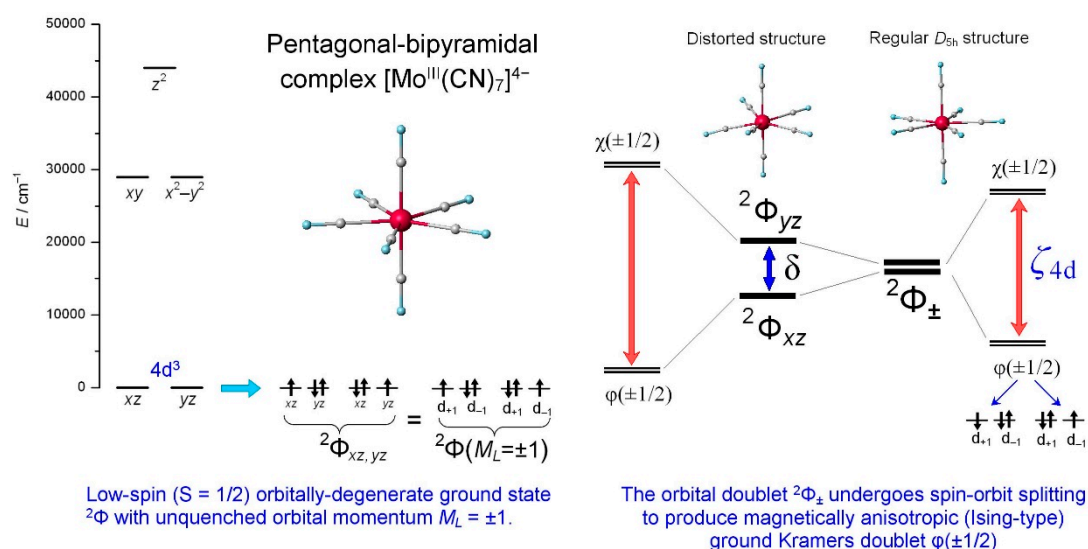


**Figure 2.** Ground-state electronic structure of the PBP  $[\text{Mo}^{\text{III}}(\text{CN})_7]^{4-}$  complex ( $D_{5h}$ ). The ligand-field energy splitting diagram of  $4d$  orbitals of  $\text{Mo}^{\text{III}}$  is indicated. Three  $4d$  electrons of  $\text{Mo}^{\text{III}}$  occupy the two lowest degenerate orbitals  $4d_{xz}$  and  $4d_{yz}$  to produce a low-spin orbital doublet  ${}^2\Phi_{xz,yz} = {}^2\Phi(M_L = \pm 1)$  with unquenched orbital momentum  $M_L = \pm 1$ . Spin-orbit coupling ( $\zeta_{4d}$ ) on  $\text{Mo}$  splits the orbital doublet  ${}^2\Phi(M_L = \pm 1)$  to produce magnetically anisotropic (Ising-type) ground Kramers doublet  $\varphi(\pm 1/2)$  and excited Kramers doublet  $\chi(\pm 1/2)$ . The orbital composition of the ground-state wave functions  $\varphi(\pm 1/2)$  is shown.

In distorted  $[\text{Mo}^{\text{III}}(\text{CN})_7]^{4-}$  complexes, the orbital momentum is reduced or quenched due to low-symmetry ligand field splitting  $\delta$  of the ground orbital doublet  ${}^2\Phi_{\pm}$ . However, weak or moderate low-symmetry distortions (when  $\delta < \zeta_{\text{Mo}}$ ) do not significantly change the overall picture,

leaving the orbital angular momentum unquenched. Moreover, these low-symmetry distortions of the  $[\text{Mo}(\text{CN})_7]^{4-}$  bipyramid do not affect the axial symmetry of the anisotropic exchange Hamiltonian  $H_{\text{eff}} = -J_{xy}(S_{\text{Mo}}^x S_{\text{V}}^x + S_{\text{Mo}}^y S_{\text{V}}^y) - J_z S_{\text{Mo}}^z S_{\text{V}}^z$  (see below).

## 2.2. Anisotropic Spin Coupling $\text{Mo}^{\text{III}}\text{-CN-V}^{\text{II}}$

Analysis of anisotropic exchange interactions between  $[\text{Mo}^{\text{III}}(\text{CN})_7]^{4-}$  complexes and  $\text{V}^{\text{II}}$  ions basically follows the theoretical model developed for  $\text{Mo}^{\text{III}}\text{-CN-Mn}^{\text{II}}$  exchange coupled pairs in  $\text{Mo}^{\text{III}}\text{Mn}^{\text{II}}_2$  SMM [47]. With the spin-orbit coupling (SOC) on  $\text{Mo}^{\text{III}}$  switched off ( $\zeta_{\text{Mo}} = 0$ ), the exchange interaction between  $\text{Mo}^{\text{III}}$  and  $\text{V}^{\text{II}}$  is described by an isotropic orbitally dependent spin Hamiltonian  $H_{\text{orb}} = A + \mathbf{R}S_{\text{Mo}}S_{\text{V}}$ , which acts in the space of the  ${}^2\Phi_{\pm}(\text{Mo}) \times {}^4A_2(\text{V})$  wave functions of the  $\text{Mo}^{\text{III}}\text{-CN-V}^{\text{II}}$  pair (with  $\times$  being the anti-symmetrized product and  ${}^4A_2(\text{V})$  the ground state of high-spin  $\text{V}^{\text{II}}$  ion). Here,  $S_{\text{Mo}}$  and  $S_{\text{V}}$  are spin operators of  $\text{Mo}^{\text{III}}$  and  $\text{V}^{\text{II}}$ , while  $A$  and  $\mathbf{R}$  are, respectively, spin-independent and spin-dependent orbital operators acting on the orbital variables only. In general case, the  $A$  and  $\mathbf{R}$  operators are written as a Hermitian  $2 \times 2$  matrices; it is noteworthy that the spin-dependent orbital  $\mathbf{R}$  matrix is diagonalized by a rotation of the coordinate frame around the polar  $z$ -axis [47]. Therefore, without loss of generality,  $H_{\text{orb}}$  can be written as

$$H_{\text{orb}} = \begin{pmatrix} A_{11} & A_{12} \\ A_{21} & A_{22} \end{pmatrix} - \begin{pmatrix} J_1 & 0 \\ 0 & J_2 \end{pmatrix} S_{\text{Mo}}S_{\text{V}}, \quad (1)$$

where  $J_1$  and  $J_2$  are orbital exchange parameters referring to the real wave functions  ${}^2\Phi_{xz} = (d_{yz})^2(d_{xz})^1$  and  ${}^2\Phi_{yz} = (d_{xz})^2(d_{yz})^1$ . Then, when the SOC on  $\text{Mo}^{\text{III}}$  is turned on, the isotropic orbitally dependent operator  $H_{\text{orb}}$  in Equation (1) transforms into an anisotropic spin Hamiltonian  $H_{\text{eff}}$  that describes effective spin coupling between the ground Kramers doublet  $\varphi(\pm 1/2)$  and the true spin  $S = 3/2$  of  $\text{V}^{\text{II}}$  ions. The spin Hamiltonian  $H_{\text{eff}}$  is obtained by projection of the full Hamiltonian  $A + \mathbf{R}S_{\text{Mo}}S_{\text{V}} + \zeta_{\text{Mo}}L_{\text{Mo}}S_{\text{Mo}}$  acting in the space of the  ${}^2\Phi_{\pm}(\text{Mo}) \times {}^4A_2(\text{V})$  wave functions onto the restricted space of the  $\varphi(m) \times {}^4A_2(\text{V})$  wave functions (where  $m = \pm 1/2$  is the projection of the fiction spin  $S = 1/2$  of the ground Kramers doublet  $\varphi(\pm 1/2)$ ). At this point it is important to emphasize a remarkable property of the pentagonal bipyramidal complex  $[\text{Mo}^{\text{III}}(\text{CN})_7]^{4-}$  that the SOC operator  $\zeta_{4d}L_{\text{Mo}}S_{\text{Mo}}$  is diagonal within the space of the  ${}^2\Phi_{\pm}(\text{Mo}) \times {}^4A_2(\text{V})$  wave functions since it does not mix the two states  ${}^2\Phi(M_L = +1)$  and  ${}^2\Phi(M_L = -1)$  of  $\text{Mo}^{\text{III}}$ ; thus the  $\zeta_{4d}L_{\text{Mo}}S_{\text{Mo}}$  operator can be replaced by its  $z$ -component  $\zeta_{4d}L_{\text{Mo}}^z S_{\text{Mo}}^z$ . This implies that the full spin Hamiltonian  $A + \mathbf{R}S_{\text{Mo}}S_{\text{V}} + \zeta_{4d}L_{\text{Mo}}^z S_{\text{Mo}}^z$  of the  $\text{Mo}^{\text{III}}\text{-CN-V}^{\text{II}}$  pair commutes with the operator  $S_{\text{Mo}}^z + S_{\text{V}}^z$  of the total spin projection on the pentagonal  $z$  axis of  $[\text{Mo}^{\text{III}}(\text{CN})_7]^{4-}$ . Thus, the projection of the total spin  $M_S(\text{Mo}) + M_S(\text{V})$  of the  $\text{Mo}^{\text{III}}\text{-CN-V}^{\text{II}}$  pair on the  $z$  axis is a good quantum number, while the total spin  $S_{\text{Mo}} + S_{\text{V}}$  is not such due to strong first-order spin-orbit coupling on  $\text{Mo}^{\text{III}}$ . Therefore, regardless of the actual symmetry of the  $\text{Mo}^{\text{III}}\text{-CN-V}^{\text{II}}$  pair (which is generally low), the effective anisotropic spin Hamiltonian  $H_{\text{eff}}$  always exhibit uniaxial symmetry, i.e.,  $-J_{xy}(S_{\text{Mo}}^x S_{\text{V}}^x + S_{\text{Mo}}^y S_{\text{V}}^y) - J_z S_{\text{Mo}}^z S_{\text{V}}^z$  (see also ref. [47] for more detail).

For the regular ( $D_{5h}$ ) or moderately distorted structure of  $[\text{Mo}^{\text{III}}(\text{CN})_7]^{4-}$ ,  $H_{\text{eff}}$  is calculated by equating the matrix elements of  $H_{\text{eff}}$  and  $A + \mathbf{R}S_{\text{Mo}}S_{\text{V}}$  in the space of wave functions  $|m, M_S\rangle = \varphi(m) \times |S_{\text{V}}, M_S\rangle, \langle m, M_S | H_{\text{eff}} | m', M_S'\rangle = \langle m, M_S | A + \mathbf{R}S_{\text{Mo}}S_{\text{V}} | m', M_S'\rangle$ . This results in

$$H_{\text{eff}} = C - J_{xy}(S_{\text{Mo}}^x S_{\text{V}}^x + S_{\text{Mo}}^y S_{\text{V}}^y) - J_z S_{\text{Mo}}^z S_{\text{V}}^z, \quad (2)$$

where  $J_z = (J_1 + J_2)/2$ ,  $J_{xy} = (J_1 - J_2)/2$ , and  $|J_1| \geq |J_2|$ ; here,  $C = (A_{11} + A_{22})/2$  is a constant stemming from the spin-independent orbital operator  $A$  in Equation (1); it can be neglected in further calculations. It is also important to note that the uniaxial symmetry of  $H_{\text{eff}}$  retains even for moderately distorted PBP  $[\text{Mo}^{\text{III}}(\text{CN})_7]^{4-}$  complexes, which frequently occur in many  $[\text{Mo}^{\text{III}}(\text{CN})_7]^{4-}$  based molecular magnets [64–66]. Indeed, the SOC operator remains diagonal ( $\zeta_{4d}L_{\text{Mo}}^z S_{\text{Mo}}^z$ ) in the

space of wave functions  ${}^2\Phi_{\pm}(\text{Mo}) \times {}^4A_2(\text{V})$ , provided that the distortions of the PBP structure of  $[\text{Mo}^{\text{III}}(\text{CN})_7]^{4-}$  slightly admix its high-lying excited  $4d^3$  states with  $M_L = \pm 2$  and  $M_L = 0$  to the ground state  ${}^2\Phi(M_L = \pm 1)$ ; in fact, due to large energy gap ( $\sim 20,000 \text{ cm}^{-1} \gg \delta$ , Figure 1), this holds true even for pronounced departures from the strict ( $D_{5h}$ ) PBP geometry of the  $[\text{Mo}^{\text{III}}(\text{CN})_7]^{4-}$  complex. At the same time, without violating the uniaxial character of the spin Hamiltonian  $H_{\text{eff}}$  in Equation (2), distortions tend to quench the orbital momentum of  $\text{Mo}^{\text{III}}$  and reduce the relative anisotropy of the  $-J_{xy}(S_{\text{Mo}}^x S_{\text{V}}^x + S_{\text{Mo}}^y S_{\text{V}}^y) - J_z S_{\text{Mo}}^z S_{\text{V}}^z$  spin Hamiltonian (which is measured by the  $J_z/J_{xy}$  ratio), especially when  $\delta > \zeta_{\text{Mo}}$ .

Thus, the uniaxial symmetry of the anisotropic exchange Hamiltonian  $H_{\text{eff}}$  is an intrinsic property of  $[\text{Mo}^{\text{III}}(\text{CN})_7]^{4-}$  complexes, which is extremely useful for creating the uniaxial symmetry of the magnetic anisotropy of SMM clusters ( $D < 0, E = 0$ ).

### 2.3. Estimate of Anisotropic Exchange Parameters

It is important to evaluate anisotropic exchange parameters  $J_z$  and  $J_{xy}$  in  $\text{Mo}^{\text{III}}\text{-CN-V}^{\text{II}}$  cyano-bridged pairs, especially given their strong impact on the barrier,  $U_{\text{eff}} \sim |J_z - J_{xy}|$  (see Figure 1) [47]. The  $\text{Mo}^{\text{III}}$  ion has diffuse and high-energy  $4d$  magnetic orbitals, which may provide strong exchange interactions with high-spin  $3d$  metal ions [54]. Especially intense exchange interactions are expected between  $[\text{Mo}^{\text{III}}(\text{CN})_7]^{4-}$  complexes and vanadium(II) ions, which, similarly to  $\text{Mo}^{\text{III}}$  ions, also tend to form strong exchange interactions due to more diffuse  $3d$  orbitals of early transition metal ions [67]. However, data on the exchange parameters in  $[\text{Mo}^{\text{III}}(\text{CN})_7]^{4-}\text{-V}^{\text{II}}$  based molecular magnets are scarce or absent [68]. The magnitude of exchange interactions in cyano-bridged pairs  $\text{Mo}^{\text{III}}\text{-CN-M}(3d)$  can be estimated from available experimental data for the related hexacyano complex  $[\text{Mo}^{\text{III}}(\text{CN})_6]^{3-}$ ,  $J = -122 \text{ cm}^{-1}$  [57] and  $J = -228 \text{ cm}^{-1}$  [58] for  $\text{Mo}^{\text{III}}\text{-CN-V}^{\text{II}}$  cyano-bridged pairs; very large exchange parameters for the  $\text{Mo}^{\text{III}}\text{-CN-V}^{\text{II}}$  linkages in a Prussian blue type structure were also predicted from a broken symmetry DFT study ( $J \approx 350 \text{ cm}^{-1}$ ) [59]. It is noteworthy, however, that these exchange parameters refer to the spin coupling between high-spin octahedral  $[\text{Mo}^{\text{III}}(\text{CN})_6]^{3-}$  complex ( $S_{\text{Mo}} = 3/2$ ) and high-spin  $\text{V}^{\text{II}}$  ions ( $S_{\text{V}} = 3/2$ ). For the  $\text{Mo}^{\text{III}}\text{-CN-V}^{\text{II}}$  pairs involving low-spin  $[\text{Mo}^{\text{III}}(\text{CN})_7]^{4-}$  PBP complex ( $S = 1/2$ ), these exchange parameters should be rescaled for a smaller spin value. Approximately, it can be done in terms of the  $t$  and  $U$  parameters of the superexchange theory, which are, respectively, electron transfer parameter between magnetic  $t_2$ -orbitals of Mo and V and metal-to-metal charge-transfer energy. With two active antiferromagnetic pathways  $4d_{xz}\text{-CN-}3d_{xz}$  and  $4d_{yz}\text{-CN-}3d_{yz}$  for the high-spin ground state  ${}^4A_2$  of  $[\text{Mo}^{\text{III}}(\text{CN})_6]^{3-}$ , this gives  $J = -8t^2/9U$  for the high-spin  $[\text{Mo}^{\text{III}}(\text{CN})_6]^{3-}$  complex; given that  $J = -228 \text{ cm}^{-1}$  [58], we have  $t^2/U = 256.5 \text{ cm}^{-1}$ , which corresponds to the electron transfer parameter of  $t \sim 3500 \text{ cm}^{-1}$  at a typical charge-transfer energy of  $U = 50,000 \text{ cm}^{-1}$  (6 eV). In the low-spin  $[\text{Mo}^{\text{III}}(\text{CN})_7]^{4-}$  PBP complex, only one active superexchange pathway lefts for each of two orbital states  ${}^2\Phi_{xz}$  and  ${}^2\Phi_{yz}$  ( $4d_{xz}\text{-CN-}3d_{xz}$  and  $4d_{yz}\text{-CN-}3d_{yz}$ , respectively), which results in two equal orbital exchange parameters  $J_1 = J_2 = -4t^2/3U$  for the linear apical  $\text{Mo}^{\text{III}}\text{-CN-V}^{\text{II}}$  pairs and  $J_1 = 4t^2/3U, J_2 \sim 0$  for the equatorial pairs (see ref. [47] for more detail). Therefore, in the linear  $\text{Mo}^{\text{III}}\text{-CN-V}^{\text{II}}$  pair, the orbital exchange parameters for the low-spin  $\text{Mo}^{\text{III}}$  ion are approximately 1.5 times larger than that for the high-spin  $\text{Mo}^{\text{III}}$ , i.e.,  $342 \text{ cm}^{-1}$  vs.  $228 \text{ cm}^{-1}$ . With the equations for the anisotropic exchange parameters,  $J_z = (J_1 + J_2)/2$  and  $J_{xy} = (J_1 - J_2)/2$ , we have antiferromagnetic Ising spin coupling for the apical pair,  $J_z = 342 \text{ cm}^{-1}$ ,  $J_{xy} = 0$ , and isotropic spin coupling  $J_z = J_{xy} = -171 \text{ cm}^{-1}$  for the equatorial pairs. However, in reality, the pairs are distorted and thus generally  $J_1$  is not equal to  $J_2$  in the apical pairs [45,47]. In further model calculations, we can conventionally assume  $J_1 = 350, J_2 = 250 \text{ cm}^{-1}$  for the orbital exchange parameters in distorted apical pairs  $\text{Mo}^{\text{III}}\text{-CN-V}^{\text{II}}$ , which corresponds to the anisotropic exchange parameters  $J_z = -300$  and  $J_{xy} = -50 \text{ cm}^{-1}$  in Equation (2). Similarly, for equatorial pairs, the isotropic exchange parameter ( $J = J_z = J_{xy}$ ) can be roughly rounded to  $-150 \text{ cm}^{-1}$ . More quantitative calculations of the exchange parameters in  $[\text{Mo}^{\text{III}}(\text{CN})_7]^{4-}$  based systems are beyond the scope of this article; they will be the subject of a separate study.

#### 2.4. Spin Energy Spectra of $\text{Mo}^{\text{III}}_k\text{V}^{\text{II}}_m$ Clusters: Engineering of High Energy Barrier

This Section presents results of a comparative study of spin energy diagrams ( $E$  vs.  $M_S$ ) for polynuclear clusters  $\text{Mo}^{\text{III}}_k\text{V}^{\text{II}}_m$  ( $k = 1-4$ ,  $m = 1-5$ ) with highly anisotropic magnetic interactions. These clusters are composed of alternating cyano-bridged  $[\text{Mo}^{\text{III}}(\text{CN})_7]^{4-}$  and  $\text{V}(\text{II})$  complexes (Figures 3–6) and involve variable number of apical and equatorial  $\text{Mo}^{\text{III}}\text{-CN-V}^{\text{II}}$  groups featuring, respectively, anisotropic (Ising-type) and isotropic exchange interactions. This study aimed to investigate the influence of the composition, structure and topology of  $\text{Mo}^{\text{III}}_k\text{V}^{\text{II}}_m$  clusters on the spin energy diagrams and, especially, on the height of the barrier  $U_{\text{eff}}$ . In this respect, it is especially interesting to investigate the dependence of the barrier on the number  $n$  of apical groups with Ising interactions, which are the main source of molecular magnetic anisotropy in  $\text{Mo}^{\text{III}}_k\text{V}^{\text{II}}_m$  clusters. For this purpose, the spin energy spectra of the  $\text{Mo}^{\text{III}}_k\text{V}^{\text{II}}_m$  clusters are calculated in terms of a spin Hamiltonian

$$\hat{H} = - \sum_{\langle ij \rangle} \left( J_{xy}(ij) (S_{\text{Mo}(i)}^x S_{\text{V}(j)}^x + S_{\text{Mo}(i)}^y S_{\text{V}(j)}^y) + J_z(ij) S_{\text{Mo}(i)}^z S_{\text{V}(j)}^z \right), \quad (3)$$

where the sum  $\langle ij \rangle$  runs over all  $\text{Mo}(i)\text{-CN-V}(j)$  pairs in the cluster; note that, since the  $\text{Mo-Mo}$  and  $\text{V-V}$  exchange interactions are neglected, here  $i$  and  $j$  indexes numerate, respectively,  $\text{Mo}$  and  $\text{V}$  centers. According to the estimates in Section 2.3, the exchange parameters are set to  $J_{xy} = -50$  and  $J_z = -300 \text{ cm}^{-1}$  for apical pairs and to  $J_{xy} = J_z = -150 \text{ cm}^{-1}$  for equatorial pairs.

Primary calculations were performed for  $\text{Mo}^{\text{III}}\text{V}^{\text{II}}_m$  clusters composed of the single central  $[\text{Mo}^{\text{III}}(\text{CN})_7]^{4-}$  complex and several  $\text{V}^{\text{II}}$  complexes attached in the apical and equatorial positions (Figures 3 and 4). It is important to note that in these clusters the projection of the total spin  $M_S$  onto the  $z$ -axis (which is parallel to the pentagonal axis of the  $[\text{Mo}^{\text{III}}(\text{CN})_7]^{4-}$  complex) is a good quantum number due to uniaxial symmetry of the spin Hamiltonian (3), which commutes with the  $S^z$  operator of the total spin. As a result, each spin quantum state has a definite  $M_S$  spin projection on the polar  $z$ -axis of  $[\text{Mo}^{\text{III}}(\text{CN})_7]^{4-}$  and thus spin energy spectra can be visualized in terms of the  $E$  vs.  $M_S$  diagrams. Figure 3 shows spin energy diagrams calculated for  $\text{Mo}^{\text{III}}\text{V}^{\text{II}}_m$  clusters with one apical pair and progressively increasing number of equatorial pairs ( $m = 1-5$ ).

In all cases (Figure 3a–d), the spin energy diagrams show a butterfly-shaped figure with a double-well profile for the lower part of the energy spectrum with doubly degenerate ground energy level represented by two spin quantum states  $M_S = +S$  and  $M_S = -S$ , which are separated by the barrier  $U_{\text{eff}}$ . Note that the spin energy diagrams of  $\text{Mo}^{\text{III}}\text{V}^{\text{II}}_m$  clusters differ considerably from the conventional double-well pattern  $DS^2$  in ordinary SMMs. In this case, similar to the parabolic energy profile  $DS^2$ , the value of the barrier  $U_{\text{eff}}$  can be associated with the energy position of the lowest spin state with the smallest spin projection (i.e.,  $M_S = 0$  or  $M_S = \pm 1/2$  for clusters with integer and half-integer spin, respectively, Figures 3 and 4). There is an interesting feature that in the  $\text{Mo}^{\text{III}}\text{V}^{\text{II}}_m$  clusters the barrier  $U_{\text{eff}}$  is rather insensitive to the number  $m$  of the equatorial  $\text{Mo-CN-V}$  pairs (with some exceptions for the smallest cluster  $\text{Mo}^{\text{III}}\text{V}^{\text{II}}_2$ , Figure 3a). This can be explained by the fact that there is the only (constant) source of the magnetic anisotropy coming from the single apical pair, while addition of the equatorial pairs with isotropic exchange interactions add nothing to the overall magnetic anisotropy  $D$  and to the barrier  $U_{\text{eff}}$ . On the other hand, albeit the barrier varies only slightly with the increasing number of equatorial  $\text{Mo}^{\text{III}}\text{-CN-V}^{\text{II}}$  pairs, the ground-state spin  $S$  increases significantly, which improves the overall SMM performance due to larger separation between the two lowest spin states  $|M_S = \pm S\rangle$  in the  $M_S$  scale.

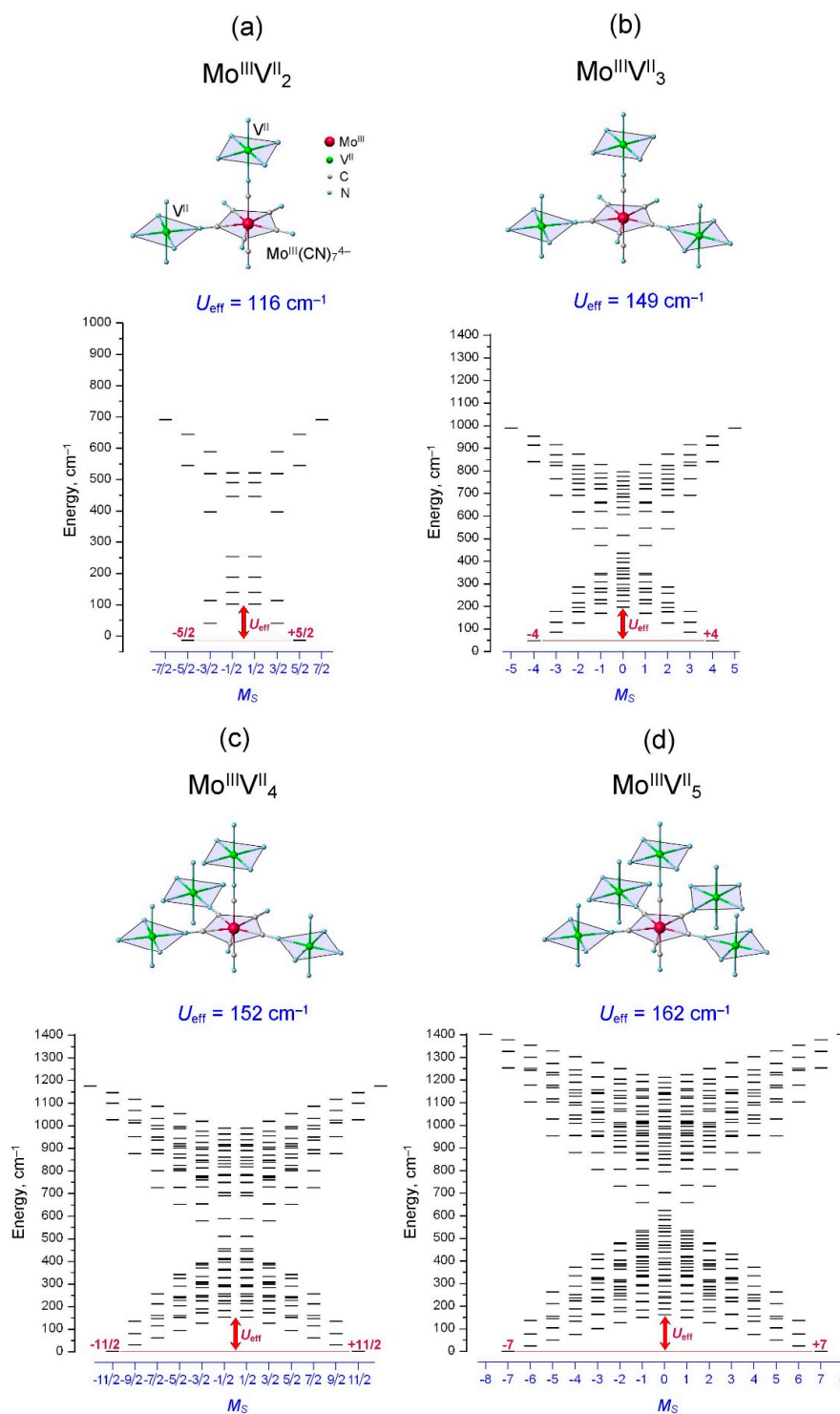


**Figure 3.** Energy diagrams of the spin levels ( $E$  vs.  $M_S$ ) of (a)  $\text{Mo}^{\text{III}}\text{V}^{\text{II}}_2$ , (b)  $\text{Mo}^{\text{III}}\text{V}^{\text{II}}_3$ , (c)  $\text{Mo}^{\text{III}}\text{V}^{\text{II}}_4$ , and (d)  $\text{Mo}^{\text{III}}\text{V}^{\text{II}}_5$  clusters with single apical group Mo–CN–V. Spin energy spectra exhibit a double-well character with doubly degenerate  $\pm M_S$  ground spin state, which is inherent in single-molecule magnets. Spin energy spectra are calculated using the anisotropic spin Hamiltonian  $H_{\text{eff}} = -J_{xy}(S_i^x S_j^x + S_i^y S_j^y) - J_z S_i^z S_j^z$  with the exchange parameters indicated in the text ( $J_z = -300 \text{ cm}^{-1}$  and  $J_{xy} = -50 \text{ cm}^{-1}$  for the apical Mo–CN–V pair and  $J_z = J_{xy} = -150 \text{ cm}^{-1}$  for equatorial pairs).

Addition of the second apical group in the  $\text{Mo}^{\text{III}}\text{V}^{\text{II}}_m$  clusters increases the barrier approximately twice (from ca.  $150$  to  $300 \text{ cm}^{-1}$ , Figure 4a–d), but the overall picture remains the same: the  $E$  vs.  $M_S$

diagrams retain a butterfly-shaped pattern with a double-well potential, the barrier  $U_{\text{eff}}$  varies rather little with increasing number  $m$  of the equatorial groups and the ground-state spin  $M_S$  increases considerably (from 5/2 to 7, Figure 4). This suggests that each apical group  $\text{Mo}^{\text{III}}\text{-CN-V}^{\text{II}}$  contributes additively to the barrier  $U_{\text{eff}}$ .

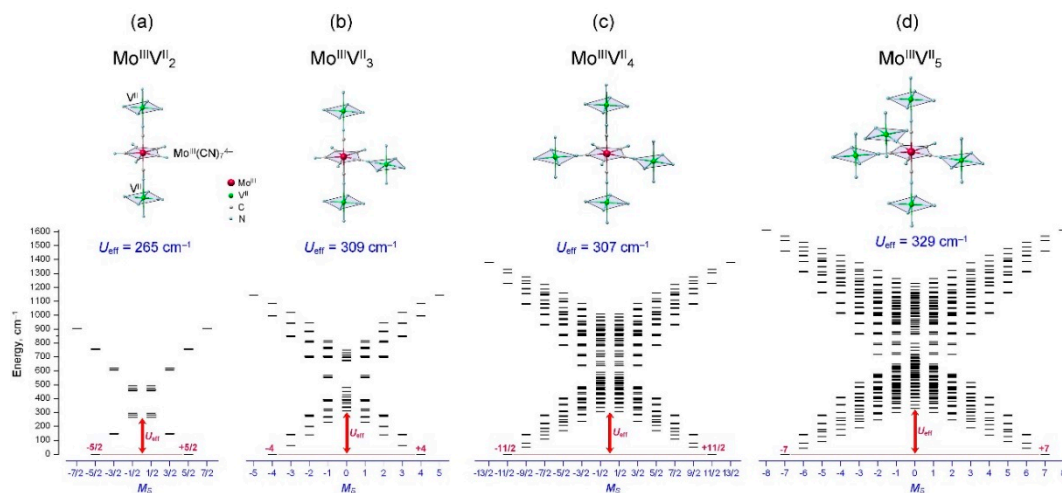


**Figure 4.** Energy diagrams of the spin levels ( $E$  vs.  $M_S$ ) of (a)  $\text{Mo}^{\text{III}}\text{V}^{\text{II}}_2$ , (b)  $\text{Mo}^{\text{III}}\text{V}^{\text{II}}_3$ , (c)  $\text{Mo}^{\text{III}}\text{V}^{\text{II}}_4$ , and (d)  $\text{Mo}^{\text{III}}\text{V}^{\text{II}}_5$  clusters with two polar  $\text{Mo-CN-V}$  groups and variable number of equatorial groups.

Next, important information on the variation of the spin energy diagrams and barrier  $U_{\text{eff}}$  on the structure of the  $\text{Mo}^{\text{III}}_k\text{V}^{\text{II}}_m$  clusters was obtained from comparative calculations for the series of  $\text{Mo}^{\text{III}}_2\text{V}^{\text{II}}_4$  clusters with the central  $\text{Mo}^{\text{III}}_2\text{V}^{\text{II}}_2$  square and two side  $\text{V}^{\text{II}}$  complexes connected via various apical and equatorial positions to the  $[\text{Mo}^{\text{III}}(\text{CN})_7]^{4-}$  complexes (Figure 5). In these calculations, an idealized structure of  $\text{Mo}^{\text{III}}_k\text{V}^{\text{II}}_m$  clusters is adopted with the parallel orientation of the local pentagonal axes of two  $[\text{Mo}^{\text{III}}(\text{CN})_7]^{4-}$  complexes to ensure uniaxial symmetry of the total spin Hamiltonian in Equation (3). In this case,  $z$ -projection  $M_S$  of the total spin is good quantum number, so each quantum spin state has a definite value of  $M_S$ .

These calculations show that all the  $\text{Mo}^{\text{III}}_2\text{V}^{\text{II}}_4$  clusters have a double-well potential with the  $M_S = \pm 5$  ground spin state and a large barrier  $U_{\text{eff}}$ , (up to  $\sim 500 \text{ cm}^{-1}$ , Figure 5b) which correlates directly with the number  $n$  of apical groups; in fact,  $U_{\text{eff}}$  is roughly proportions to  $n$  (Figure 5). Similar regularities were also found for larger  $\text{Mo}^{\text{III}}_4\text{V}^{\text{II}}_4$  clusters with cubic and ladder structures (Figure 6). Thus, in the ladder cluster  $\text{Mo}^{\text{III}}_4\text{V}^{\text{II}}_4$  with six apical  $\text{Mo-CN-V}$  groups ( $n = 6$ ), the barrier reaches a value of  $U_{\text{eff}} = 741 \text{ cm}^{-1}$ . Consequently, these results indicate the possibility of further increase of the barrier in larger  $\text{Mo}^{\text{III}}_k\text{V}^{\text{II}}_m$  clusters with alternating  $[\text{Mo}^{\text{III}}(\text{CN})_7]^{4-}$  and  $\text{V}^{\text{II}}$  units, in which the number  $n$  of apical groups may be considerably larger.

To establish a more quantitative correlation between  $U_{\text{eff}}$  and anisotropic exchange parameters, numerous calculations were performed for various  $\text{Mo}^{\text{III}}_k\text{V}^{\text{II}}_m$  clusters with variable exchange parameters  $J_z$  and  $J_{xy}$  for the apical and equatorial  $\text{Mo}^{\text{III}}\text{-CN-V}^{\text{II}}$  groups. Analysis of these results has revealed that the barrier is approximately given by  $U_{\text{eff}} \sim 0.5 |J_z - J_{xy}| n$ , provided that the isotropic exchange interactions (i.e., with  $J_z = J_{xy}$ ) for the equatorial pairs are strong enough as compared to the anisotropic Ising-type exchange interactions in the apical pairs ( $J_z > J_{xy}$ ). The meaning of this condition is that the isotropic exchange interactions of equatorial pairs integrate the local magnetic anisotropies of the apical pairs into the overall magnetic anisotropy of the  $\text{Mo}^{\text{III}}_k\text{V}^{\text{II}}_m$  cluster, and thus they must be strong enough to carry out this function. Fortunately, for the specific cyano-bridged  $\text{Mo}^{\text{III}}_k\text{V}^{\text{II}}_m$  clusters, this condition is well satisfied due to the relation between anisotropic exchange parameters ( $J_z$ ,  $J_{xy}$ ) and orbital exchange parameters  $J_1, J_2$  involved in the orbitally-dependent spin Hamiltonian (2),  $J_z = (J_1 + J_2)/2$  and  $J_{xy} = (J_1 - J_2)/2$ .

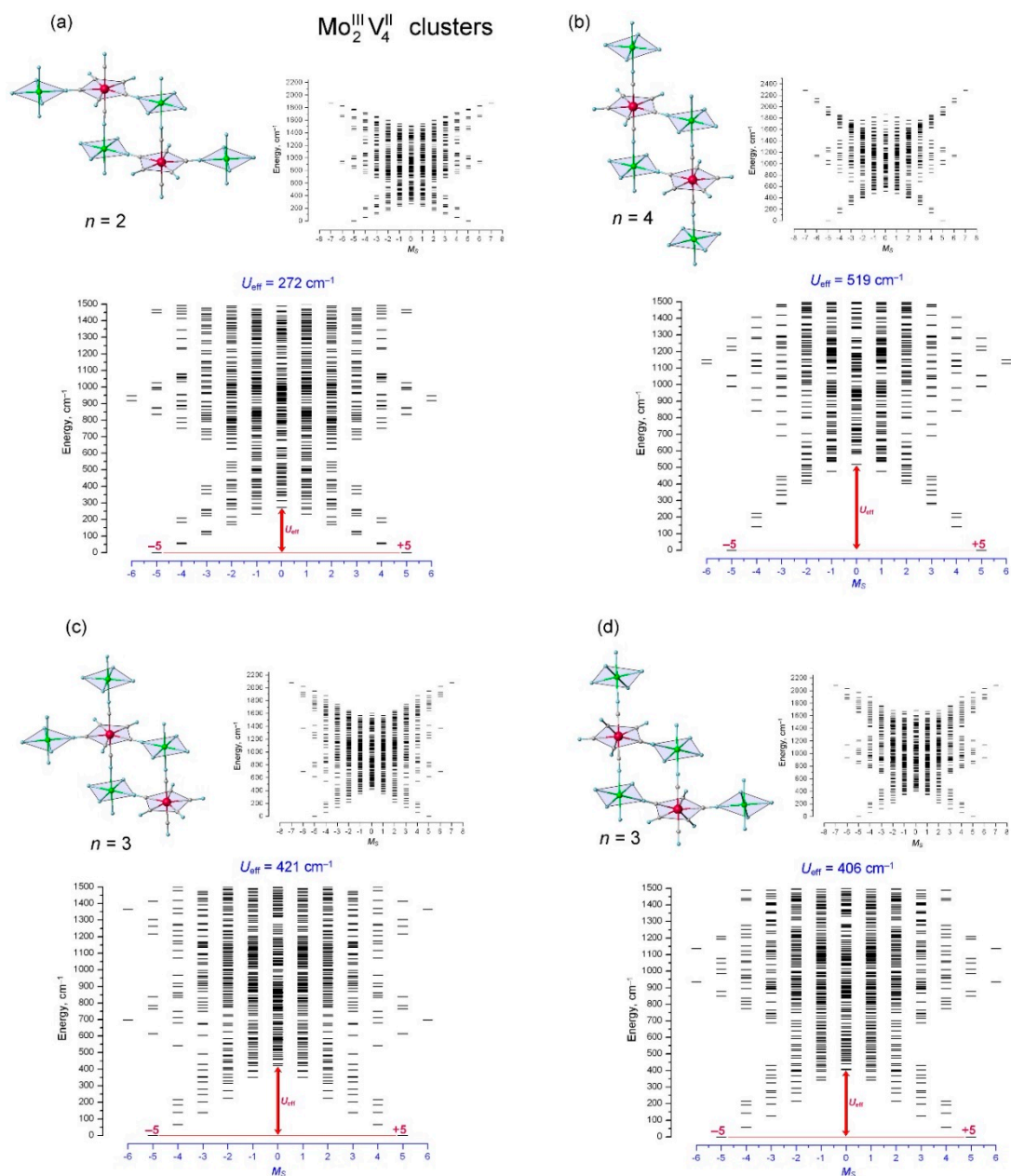


**Figure 5.** Energy diagrams of the spin levels ( $E$  vs.  $M_S$ ) of four Mo<sup>III</sup><sub>2</sub>V<sup>II</sup><sub>4</sub> clusters with the different number  $n$  of apical Mo–CN–V groups, (a)  $n = 2$ , (b)  $n = 4$ , (c,d)  $n = 3$ . The full spin energy diagrams are depicted in the inserts. The height of the barrier  $U_{\text{eff}}$  correlates directly with the number  $n$  of apical Mo–CN–V groups.

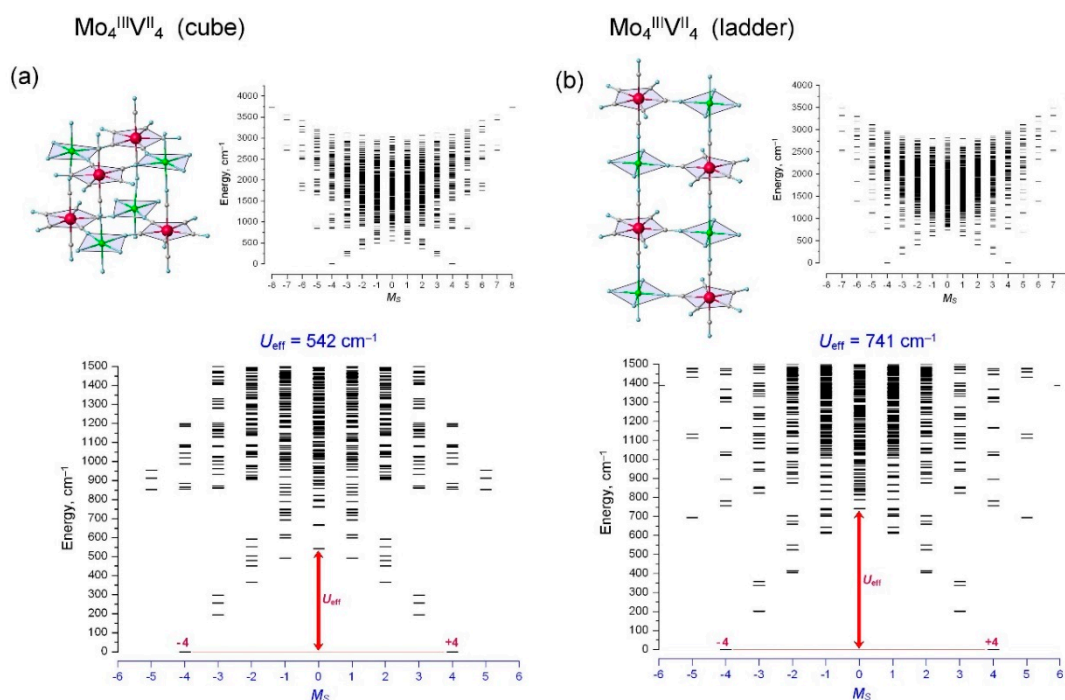


**Figure 6.** Energy diagrams of the spin levels ( $E$  vs.  $M_S$ ) of  $\text{Mo}_4^{\text{III}}\text{V}_4^{\text{II}}$  clusters with (a) four (cube,  $n = 4$ ) and (b) with six (ladder,  $n = 6$ ) apical Mo–CN–V groups calculated using anisotropic spin Hamiltonian (3) with the exchange parameters indicated in the text.

These data indicate the possibility of the direct scaling of the barrier  $U_{\text{eff}}$  in molecular cyano-bridged clusters based on alternating  $[\text{Mo}^{\text{III}}(\text{CN})_7]^{4-}$  and  $\text{V}^{\text{II}}$  complexes by means of increasing the cluster size and proper organization of its structure and composition. In principle, from the ratio  $U_{\text{eff}} \sim 0.5 |J_z - J_{xy}| n$  with  $|J_z - J_{xy}| = 200\text{--}300 \text{ cm}^{-1}$ , one can expect to obtain a barrier above  $1000 \text{ cm}^{-1}$  in large  $\text{Mo}_k^{\text{III}}\text{V}_m^{\text{II}}$  clusters. The main conditions for obtaining a high barrier are a large number  $n$  of apical groups and large absolute values of the anisotropic exchange parameters  $J_z$  and  $J_{xy}$ . However, it is important to note that, in the large polynuclear  $\text{Mo}_k^{\text{III}}\text{V}_m^{\text{II}}$  clusters with a fixed number of apical groups  $n$ , the maximum barrier  $U_{\text{eff}}$  could be obtained only if there are a sufficient number of equatorial groups in the cluster. Thus, the equatorial  $\text{Mo}^{\text{III}}\text{--CN--V}^{\text{II}}$  groups carry out an important function in the formation of a high barrier: although their isotropic exchange interactions do not directly contribute to the magnetic anisotropy of the  $\text{Mo}_k^{\text{III}}\text{V}_m^{\text{II}}$  cluster, they ensure the overall magnetic connectivity of the molecular spin cluster and thus help to convert the local Ising-type exchange anisotropy  $-J_{xy}(S_i^x S_j^x + S_i^y S_j^y) - J_z S_i^z S_j^z$  of individual apical pairs  $\text{Mo}^{\text{III}}\text{--CN--V}^{\text{II}}$  into the value of the barrier  $U_{\text{eff}}$ .

A unique feature of the PBP  $[\text{Mo}^{\text{III}}(\text{CN})_7]^{4-}$  complexes as molecular building blocks lies in the fact that their uniaxial anisotropic exchange interactions  $-J_{xy}(S_i^x S_j^x + S_i^y S_j^y) - J_z S_i^z S_j^z$  automatically create a molecular magnetic anisotropy  $D$  with a purely axial symmetry, without undesirable transverse component ( $E = 0$ ), which is very important for obtaining a high barrier  $U_{\text{eff}}$ . In other words, the symmetry of the molecular magnetic anisotropy is higher than the geometric symmetry of the molecule. This simplifies drastically the problem of molecular design of nanomagnets, since it eliminates the need to obtain the axial geometric symmetry of a SMM cluster during its chemical synthesis.

However, it is important to note that this study does not fully address the problem of designing high-temperature SMMs—its goal is to demonstrate theoretically a great potential of the new approach in engineering high energy barriers  $U_{\text{eff}}$ , which exploits highly anisotropic exchange interactions of PBP  $[\text{Mo}^{\text{III}}(\text{CN})_7]^{4-}$  complexes. Of course, many complicated features of these systems (such as distortions, non-collinear orientation of magnetic axes, specific molecular building blocks and structures, synthetic approaches, etc.) remain so far beyond the limits of this theoretical model. Thus, the paper discusses

some new general principles for constructing a high barrier rather than specific recommendations for the synthesis of advanced SMM. Practical development of this strategy will be based on new PBP 4d and 5d complexes with unquenched orbital momentum (instead of  $[\text{Mo}^{\text{III}}(\text{CN})_7]^{4-}$  and  $[\text{Re}^{\text{IV}}(\text{CN})_7]^{3-}$  heptacyanide complexes), in which the pentagonal coordination of the metal ion in the equatorial plane is enforced by a five-membered chelate ring of the planar pentadentate macrocyclic ligands (see our recent paper [69]); this work is underway.

### 3. Method and Computation Details

Spin energy spectra of  $\text{Mo}^{\text{III}}_k\text{V}^{\text{II}}_m$  clusters were calculated using specially designed computational approaches and routines based of anisotropic spin Hamiltonian in Equation (3). More specifically, a Fortran routine first calculates the set of matrix elements of the spin exchange Hamiltonian (3) in the full basis set of multicenter spin functions generated by the product of single-ion spin functions of Mo(III) and V(II) ions involved in the  $\text{Mo}_k\text{V}_m$  cluster. Next, the energies of spin states and eigenvectors are obtained by diagonalization of the full matrix of the spin Hamiltonian (3); then, the eigenvectors are sorted according their  $E$  energies and  $M_S$  spin projections to visualize the spin energy diagrams shown in Figures 3–6.

### 4. Conclusions

In summary, anisotropic Ising-type exchange interactions  $-J_{xy}(S_i^x S_j^x + S_i^y S_j^y) - J_z S_i^z S_j^z$  with large exchange parameters  $J_z$  and  $J_{xy}$  generated by PBP  $[\text{Mo}^{\text{III}}(\text{CN})_7]^{4-}$  complexes and  $\text{V}^{\text{II}}$  ions connected via apical positions represent a very efficient tool for constructing high-performance SMMs. It is shown that in mixed 4d–3d heterometallic SMM clusters composed of alternating  $[\text{Mo}^{\text{III}}(\text{CN})_7]^{4-}$  and  $\text{V}^{\text{II}}$  complexes the spin-reversal barrier is controlled by anisotropic exchange parameters and the number  $n$  of apical  $\text{Mo}^{\text{III}}\text{–CN–V}^{\text{II}}$  groups,  $U_{\text{eff}} \sim 0.5 |J_z - J_{xy}| n$ . This finding provides a very efficient straightforward strategy for scaling  $U_{\text{eff}}$  and  $T_B$  values by means of enhancing exchange parameters  $J$  and  $J_{xy}$  and increasing the number of PBP  $[\text{Mo}^{\text{III}}(\text{CN})_7]^{4-}$  complexes in a SMM molecule. Some ideas on molecular engineering high energy barrier  $U_{\text{eff}}$  and further developments toward high- $T$  SMMs are discussed, which are illustrated in Figures 3–6. Practical implementation of this approach will be focused on a new family of PBP 4d and 5d complexes with pentadentate macrocyclic ligands [69].

**Acknowledgments:** This work was partially supported by the Russian Foundation for Basic Research (Project 18-03-00543a) and partially supported by the Federal Agency of Scientific Organizations (Agreement No 007-GZ/CH3363/26) in part of development of computational methods.

**Conflicts of Interest:** The author declares no conflict of interest.

### References

1. Sessoli, R.; Gatteschi, D.; Caneschi, A.; Novak, M.A. Magnetic bistability in a metal-ion cluster. *Nature* **1993**, *365*, 141–143. [[CrossRef](#)]
2. Sessoli, R.; Tsai, H.L.; Schake, A.R.; Wang, S.Y.; Vincent, J.B.; Foltling, K.; Gatteschi, D.; Christou, G.; Hendrickson, D.N. High-spin molecules:  $[\text{Mn}_{12}\text{O}_{12}(\text{O}_2\text{CR})_{16}(\text{H}_2\text{O})_4]$ . *J. Am. Chem. Soc.* **1993**, *115*, 1804–1816. [[CrossRef](#)]
3. Gatteschi, D.; Sessoli, R. Quantum tunneling of magnetization and related phenomena in molecular materials. *Angew. Chem. Int. Ed.* **2003**, *42*, 268–297. [[CrossRef](#)] [[PubMed](#)]
4. Coulon, C.; Miyasaka, H.; Clérac, R. Single-Molecule Magnets and Related Phenomena. In *Structure and Bonding*; Winpenny, R., Ed.; Springer: Berlin, Germany, 2006; Volume 122.
5. Gatteschi, D.; Sessoli, R.; Villain, J. *Molecular Nanomagnets*; Oxford University Press: Oxford, UK, 2006.
6. Gao, S. *Molecular Nanomagnets and Related Phenomena*; Springer: New York, NY, USA, 2015; Volume 164.
7. Milios, C.J.; Winpenny, R.E.P. Cluster-based single-molecule magnets. In *Molecular Nanomagnets and Related Phenomena*; Gao, S., Ed.; Springer: Berlin, Germany, 2015; Volume 164, pp. 1–109.
8. Ardavan, A.; Blundell, S.J. Storing quantum information in chemically engineered nanoscale magnets. *J. Mater. Chem.* **2009**, *19*, 1754–1760. [[CrossRef](#)]

9. Leuenberger, M.N.; Loss, D. Quantum computing in molecular magnets. *Nature* **2001**, *410*, 789–793. [[CrossRef](#)] [[PubMed](#)]
10. Aromi, G.; Aguilà, D.; Gamez, P.; Luis, F.; Roubeau, O. Design of magnetic coordination complexes for quantum computing. *Chem. Soc. Rev.* **2012**, *41*, 537–546. [[CrossRef](#)] [[PubMed](#)]
11. Wedge, C.J.; Timco, G.A.; Spielberg, E.T.; George, R.E.; Tuna, F.; Rigby, S.; McInnes, E.J.L.; Winpenny, R.E.P.; Blundell, S.J.; Ardavan, A. Chemical engineering of molecular qubits. *Phys. Rev. Lett.* **2012**, *108*, 107204. [[CrossRef](#)] [[PubMed](#)]
12. Pedersen, K.S.; Ariciu, A.; McAdams, S.; Weihe, H.; Bendix, J.; Tuna, F.; Piligkos, S. Toward Molecular 4f Single-Ion Magnet Qubits. *J. Am. Chem. Soc.* **2016**, *138*, 5801–5804. [[CrossRef](#)] [[PubMed](#)]
13. Rocha, A.R.; García-Suarez, V.M.; Bailey, S.W.; Lambert, C.J.; Ferrer, J.; Sanvito, S. Towards Molecular Spintronics. *Nat. Mater.* **2005**, *4*, 335–339. [[CrossRef](#)] [[PubMed](#)]
14. Bogani, L.; Wernsdorfer, W. Molecular spintronics using single-molecule magnets. *Nat. Mater.* **2008**, *7*, 179–186. [[CrossRef](#)] [[PubMed](#)]
15. Waldmann, O. A criterion for the anisotropy barrier in single-molecule magnets. *Inorg. Chem.* **2007**, *46*, 10035–10037. [[CrossRef](#)] [[PubMed](#)]
16. Ruiz, E.; Cirera, J.; Cano, J.; Alvarez, S.; Loose, C.; Kortus, J. Can large magnetic anisotropy and high spin really coexist? *Chem. Commun.* **2008**, *1*, 52–54. [[CrossRef](#)]
17. Neese, F.; Pantazis, D.A. What is not required to make a single molecule magnet. *Faraday Discuss.* **2011**, *148*, 229–238. [[CrossRef](#)] [[PubMed](#)]
18. Sessoli, R.; Powell, A.K. Strategies towards single molecule magnets based on lanthanide ions. *Coord. Chem. Rev.* **2009**, *253*, 2328–2341. [[CrossRef](#)]
19. Sorace, L.; Benelli, J.R.; Gatteschi, D. Lanthanides in molecular magnetism: old tools in a new field. *Chem. Soc. Rev.* **2011**, *40*, 3092–3105. [[CrossRef](#)] [[PubMed](#)]
20. Rinehart, J.D.; Long, J.R. Exploiting single-ion anisotropy in the design of f-element single-molecule magnets. *Chem. Sci.* **2011**, *2*, 2078–2085. [[CrossRef](#)]
21. Layfield, R.A.; Murugesu, M. *Lanthanides and Actinides in Molecular Magnetism*; Wiley-VCH: Weinheim, Germany, 2015.
22. Ishikawa, N.; Sugita, M.; Ishikawa, T.; Koshihara, S.; Kaizu, Y. Lanthanide double-decker complexes functioning as magnets at the single-molecular level. *J. Am. Chem. Soc.* **2003**, *125*, 8694–8695. [[CrossRef](#)] [[PubMed](#)]
23. Luzon, J.; Sessoli, R. Lanthanides in molecular magnetism: So fascinating, so challenging. *Dalton Trans.* **2012**, *41*, 13556–13567. [[CrossRef](#)] [[PubMed](#)]
24. Woodruff, D.N.; Winpenny, R.E.P.; Layfield, R.A. Lanthanide Single-Molecule Magnets. *Chem. Rev.* **2013**, *113*, 5110–5148. [[CrossRef](#)] [[PubMed](#)]
25. Layfield, R.A. Organometallic single-molecule magnets. *Organometallics* **2014**, *33*, 1084–1099. [[CrossRef](#)]
26. Tang, J.; Zhang, P. *Lanthanide Single-Molecule Magnets*; Springer: Berlin, Germany, 2015.
27. Liddle, S.T.; van Slageren, J. Improving f-element single molecule magnets. *Chem. Soc. Rev.* **2015**, *44*, 6655–6669. [[CrossRef](#)] [[PubMed](#)]
28. Habib, F.; Murugesu, M. Lessons learned from dinuclear lanthanide nano-magnets. *Chem. Soc. Rev.* **2013**, *42*, 3278–3288. [[CrossRef](#)] [[PubMed](#)]
29. Rinehart, J.D.; Fang, M.; Evans, W.J.; Long, J.R. A N<sub>2</sub><sup>3-</sup>Radical-Bridged Terbium Complex Exhibiting Magnetic Hysteresis at 14 K. *J. Am. Chem. Soc.* **2011**, *133*, 14236–14239. [[CrossRef](#)] [[PubMed](#)]
30. Chen, Y.-C.; Liu, J.-L.; Ungur, L.; Liu, J.; Li, Q.-W.; Wang, L.-F.; Ni, Z.-P.; Chibotaru, L.F.; Chen, X.-M.; Tong, M.-L. Symmetry-Supported Magnetic Blocking at 20 K in Pentagonal Bipyramidal Dy(III) Single-Ion Magnets. *J. Am. Chem. Soc.* **2016**, *138*, 2829–2837. [[CrossRef](#)] [[PubMed](#)]
31. Ding, Y.S.; Chilton, N.F.; Winpenny, R.E.P.; Zheng, Y.Z. On Approaching the Limit of Molecular Magnetic Anisotropy: A Near-Perfect Pentagonal Bipyramidal Dysprosium(III) Single-Molecule Magnet. *Angew. Chem. Int. Ed.* **2016**, *55*, 16071–16074. [[CrossRef](#)] [[PubMed](#)]
32. Guo, F.S.; Day, B.M.; Chen, Y.C.; Tong, M.L.; Mansikkamäki, A.; Layfield, R.A. A dysprosium metallocene single-molecule magnet functioning at the axial limit. *Angew. Chem. Int. Ed.* **2017**, *56*, 11445–11449. [[CrossRef](#)] [[PubMed](#)]
33. Goodwin, C.A.P.; Ortu, F.; Reta, D.; Chilton, N.F.; Mills, D.P. Molecular magnetic hysteresis at 60 kelvin in dysprosocenium. *Nature* **2017**, *548*, 439–442. [[CrossRef](#)] [[PubMed](#)]

34. Milios, C.J.; Vinslava, A.; Wernsdorfer, W.; Moggach, S.; Parsons, S.; Perlepes, S.P.; Christou, G.; Brechin, E.K. A record Anisotropy Barrier for a Single-molecule Magnet. *J. Am. Chem. Soc.* **2007**, *129*, 2754–2755. [[CrossRef](#)] [[PubMed](#)]
35. Craig, G.A.; Murrie, M. 3D single-ion magnets. *Chem. Soc. Rev.* **2015**, *44*, 2135–2147. [[CrossRef](#)] [[PubMed](#)]
36. Frost, J.M.; Harriman, K.L.M.; Murugesu, M. The rise of 3-d single-ion magnets in molecular magnetism: Towards materials from molecules. *Chem. Sci.* **2016**, *7*, 2470–2491. [[CrossRef](#)] [[PubMed](#)]
37. Zadrozny, J.M.; Xiao, D.J.; Long, J.R.; Atanasov, M.; Neese, F.; Grandjean, F.; Long, G.J. Mossbauer Spectroscopy as a Probe of Magnetization Dynamics in the Linear Iron(I) and Iron(II) Complexes  $[\text{Fe}(\text{C}(\text{SiMe}_3)_3)_2]^{1-/\text{0}}$ . *Inorg. Chem.* **2013**, *52*, 13123–13131. [[CrossRef](#)] [[PubMed](#)]
38. Yao, X.-N.; Du, J.-Z.; Zhang, Y.-Q.; Leng, X.-B.; Yang, M.-W.; Jiang, S.-D.; Wang, Z.-X.; Ouyang, Z.-W.; Deng, L.; Wang, B.-W.; et al. Two-Coordinate Co(II) Imido Complexes as Outstanding Single-Molecule Magnets. *J. Am. Chem. Soc.* **2017**, *139*, 373–380. [[CrossRef](#)] [[PubMed](#)]
39. Bar, A.K.; Pichon, C.; Sutter, J.-P. Magnetic anisotropy in two- to eight-coordinated transition–metal complexes: Recent developments in molecular magnetism. *Coord. Chem. Rev.* **2016**, *308*, 346–380. [[CrossRef](#)]
40. Ruamps, R.; Batchelor, L.J.; Guillot, R.; Zakhia, G.; Barra, A.L.; Wernsdorfer, W.; Guihéry, N.; Mallah, T. Ising-type magnetic anisotropy and single molecule magnet behaviour in mononuclear trigonal bipyramidal Co(II) complexes. *Chem. Sci.* **2014**, *5*, 3418–3424. [[CrossRef](#)]
41. Ruamps, R.; Maurice, R.; Batchelor, L.J.; Boggio-Pasqua, M.; Guillot, R.; Barra, A.L.; Liu, J.; Bendeif, E.-E.; Pillet, S.; Hill, S.; et al. Giant Ising-Type Magnetic Anisotropy in Trigonal Bipyramidal Ni(II) Complexes: Experiment and Theory. *J. Am. Chem. Soc.* **2013**, *135*, 3017–3026. [[CrossRef](#)] [[PubMed](#)]
42. Novikov, V.V.; Pavlov, A.A.; Nelyubina, Y.V.; Boulon, M.-E.; Varzatskii, O.A.; Voloshin, Y.Z.; Winpenny, R.E.P. A Trigonal Prismatic Mononuclear Cobalt(II) Complex Showing Single-Molecule Magnet Behavior. *J. Am. Chem. Soc.* **2015**, *137*, 9792–9795. [[CrossRef](#)] [[PubMed](#)]
43. Morrison, C.A.; Leavitt, R.P. Spectroscopic Properties of Triply Ionized Lanthanides in Transparent Host Crystals. In *Handbook on the Physics and Chemistry of Rare Earths*; Elsevier: Amsterdam, The Netherlands, 1982; Volume 5, pp. 461–692.
44. Ungur, L.; Chibotaru, L.F. Strategies toward High-Temperature Lanthanide-Based Single-Molecule Magnets. *Inorg. Chem.* **2016**, *55*, 10043–10056. [[CrossRef](#)] [[PubMed](#)]
45. Mironov, V.S.; Chibotaru, L.F.; Ceulemans, A. Mechanism of a Strongly Anisotropic  $\text{Mo}^{\text{III}}\text{–CN–Mn}^{\text{II}}$  Spin–Spin Coupling in Molecular Magnets Based on the  $[\text{Mo}(\text{CN})_7]^{4-}$  Heptacyanomolybdate: A New Strategy for Single-Molecule Magnets with High Blocking Temperatures. *J. Am. Chem. Soc.* **2003**, *125*, 9750–9760. [[CrossRef](#)] [[PubMed](#)]
46. Mironov, V.S. New approaches to the problem of high-temperature single-molecule magnets. *Dokl. Phys. Chem.* **2006**, *408*, 130–136. [[CrossRef](#)]
47. Mironov, V.S. Origin of Dissimilar Single-Molecule Magnet Behavior of Three  $\text{Mn}^{\text{II}}\text{Mo}^{\text{III}}$  Complexes Based on  $[\text{Mo}^{\text{III}}(\text{CN})_7]^{4-}$  Heptacyanomolybdate: Interplay of  $\text{Mo}^{\text{III}}\text{–CN–Mn}^{\text{II}}$  Anisotropic Exchange Interactions. *Inorg. Chem.* **2015**, *54*, 11339–11355. [[CrossRef](#)] [[PubMed](#)]
48. Bennett, M.V.; Long, J.R. New Cyanometalate Building Units: Synthesis and Characterization of  $[\text{Re}(\text{CN})_7]^{3-}$  and  $[\text{Re}(\text{CN})_8]^{3-}$ . *J. Am. Chem. Soc.* **2003**, *125*, 2394–2395. [[CrossRef](#)] [[PubMed](#)]
49. Samsonenko, D.G.; Paulsen, C.; Lhotel, E.; Mironov, V.S.; Vostrikova, K.E.  $[\text{Mn}^{\text{III}}(\text{Schiff base})_3[\text{Re}^{\text{IV}}(\text{CN})_7]$ , highly anisotropic 3D coordination framework: Synthesis, crystal structure, magnetic investigations, and theoretical analysis. *Inorg. Chem.* **2014**, *53*, 10217–10231. [[CrossRef](#)] [[PubMed](#)]
50. Bendix, J.; Steenberg, P.; Sotofte, I. Isolation and Molecular Structure of Hexacyanoruthenate(III). *Inorg. Chem.* **2003**, *42*, 4510–4512. [[CrossRef](#)] [[PubMed](#)]
51. Albores, P.; Slep, L.D.; Baraldo, L.M.; Baggio, R.; Garland, M.T.; Rentschler, E. Crystal Structure and Electronic and Magnetic Properties of Hexacyanoosmate(III). *Inorg. Chem.* **2006**, *45*, 2361–2363. [[CrossRef](#)] [[PubMed](#)]
52. Mironov, V.S. Trigonal bipyramidal spin clusters with orbitally degenerate 5d cyano complexes  $[\text{Os}^{\text{III}}(\text{CN})_6]^{3-}$ , prototypes of high-temperature single-molecule magnets. *Dokl. Phys. Chem.* **2007**, *415*, 199–204. [[CrossRef](#)]
53. Dreiser, J.; Pedersen, K.S.; Schnegg, A.; Holldack, K.; Nehrkor, J.; Sigrist, M.; Tregenna-Piggott, P.; Mutka, H.; Weihe, H.; Mironov, V.S.; et al. Three-Axis Anisotropic Exchange Coupling in the Single-Molecule Magnets  $\text{NEt}_4[\text{Mn}^{\text{III}}_2(5\text{-Brsalen})_2(\text{MeOH})_2\text{M}^{\text{III}}(\text{CN})_6]$  (M = Ru, Os). *Chem. Eur. J.* **2013**, *19*, 3693–3701. [[CrossRef](#)] [[PubMed](#)]

54. Wang, X.-Y.; Avendaño, C.; Dunbar, K.R. Molecular magnetic materials based on 4d and 5d transition metals. *Chem. Soc. Rev.* **2011**, *40*, 3213–3238. [[CrossRef](#)] [[PubMed](#)]
55. Qian, K.; Huang, X.-C.; Zhou, C.; You, X.-Z.; Wang, X.-Y.; Dunbar, K.R. A Single-Molecule Magnet Based on Heptacyanomolybdate with the Highest Energy Barrier for a Cyanide Compound. *J. Am. Chem. Soc.* **2013**, *135*, 13302–13305. [[CrossRef](#)] [[PubMed](#)]
56. Wu, D.-Q.; Shao, D.; Wei, X.-Q.; Shen, F.-X.; Shi, L.; Kempe, D.; Zhang, Y.-Z.; Dunbar, K.R.; Wang, X.-Y. Reversible On–Off Switching of a Single-Molecule Magnet via a Crystal-to-Crystal Chemical Transformation. *J. Am. Chem. Soc.* **2017**, *139*, 11714–11717. [[CrossRef](#)] [[PubMed](#)]
57. Freedman, D.E.; Jenkins, D.M.; Long, J.R. Strong magnetic exchange coupling in the cyano-bridged coordination clusters  $[(\text{PY5Me}_2)_4\text{V}_4\text{M}(\text{CN})_6]^{5+}$  (M = Cr, Mo). *Chem. Commun.* **2009**, 4829–4831. [[CrossRef](#)] [[PubMed](#)]
58. Pinkowicz, D.; Southerland, H.; Wang, X.-Y.; Dunbar, K.R. Record Antiferromagnetic Coupling for a 3d/4d Cyanide-Bridged Compound. *J. Am. Chem. Soc.* **2014**, *136*, 9922–9924. [[CrossRef](#)] [[PubMed](#)]
59. Ruiz, E.; Rodríguez-Fortea, A.; Alvarez, S.; Verdaguier, M. Is it possible to get high  $T_c$  magnets with prussian blue analogues? A theoretical prospect. *Chem. Eur. J.* **2005**, *11*, 2135–2144. [[CrossRef](#)] [[PubMed](#)]
60. Gunter, M.J.; Berry, K.J.; Murray, K.S. A Model for the Cyanide Form of Oxidized Cytochrome Oxidase: An Iron(III)/Copper(II) Porphyrin Complex Displaying Ferromagnetic Coupling. *J. Am. Chem. Soc.* **1984**, *106*, 4227–4235. [[CrossRef](#)]
61. Langley, S.K.; Wielechowski, D.P.; Vieru, V.; Chilton, N.F.; Moubaraki, B.; Abrahams, B.F.; Chibotaru, L.F.; Murray, K.S. A  $\{\text{Cr}^{\text{III}}_2\text{Dy}^{\text{III}}_2\}$  Single-Molecule Magnet: Enhancing the Blocking Temperature through 3d Magnetic Exchange. *Angew. Chem. Int. Ed.* **2013**, *52*, 12014–12019. [[CrossRef](#)] [[PubMed](#)]
62. Langley, S.K.; Wielechowski, D.P.; Vieru, V.; Chilton, N.F.; Moubaraki, B.; Chibotaru, L.F.; Murray, K.S. Modulation of slow magnetic relaxation by tuning magnetic exchange in  $\{\text{Cr}_2\text{Dy}_2\}$  single molecule magnets. *Chem. Sci.* **2014**, *5*, 3246–3256. [[CrossRef](#)]
63. Hursthouse, M.B.; Maijk, K.M.A.; Soares, A.M.; Gibson, J.F.; Griffith, W.P. The X-ray crystal structure of  $\text{NaK}_3[\text{Mo}(\text{CN})_7] \cdot 2\text{H}_2\text{O}$  and the structure of its anion in aqueous solution. *Inorg. Chim. Acta* **1980**, *45*, L81–L82. [[CrossRef](#)]
64. Larionova, J.; Clérac, R.; Sanchiz, J.; Kahn, O.; Golhen, S.; Ouahab, L. Ferromagnetic Ordering, Anisotropy, and Spin Reorientation for the Cyano-Bridged Bimetallic Compound  $\text{Mn}_2(\text{H}_2\text{O})_5\text{Mo}(\text{CN})_7 \cdot 4\text{H}_2\text{O}$  ( $\alpha$  Phase). *J. Am. Chem. Soc.* **1998**, *120*, 13088–13095. [[CrossRef](#)]
65. Larionova, J.; Kahn, O.; Gohlen, S.; Ouahab, L.; Clérac, R. Structure, Ferromagnetic Ordering, Anisotropy, and Spin Reorientation for the Two-Dimensional Cyano-Bridged Bimetallic Compound  $\text{K}_2\text{Mn}_3(\text{H}_2\text{O})_6[\text{Mo}(\text{CN})_7]_2 \cdot 6\text{H}_2\text{O}$ . *J. Am. Chem. Soc.* **1999**, *121*, 3349–3356. [[CrossRef](#)]
66. Wang, Q.-L.; Southerland, H.; Li, J.-R.; Prosvirin, A.V.; Zhao, H.; Dunbar, K.R. Crystal-to-Crystal Transformation of Magnets Based on Heptacyanomolybdate(III) Involving Dramatic Changes in Coordination Mode and Ordering Temperature. *Angew. Chem. Int. Ed.* **2012**, *51*, 9321–9324. [[CrossRef](#)] [[PubMed](#)]
67. Holmes, S.M.; Girolami, G.S. Sol–Gel Synthesis of  $\text{KV}^{\text{II}}[\text{Cr}^{\text{III}}(\text{CN})_6] \cdot 2\text{H}_2\text{O}$ : A Crystalline Molecule-Based Magnet with a Magnetic Ordering Temperature above 100 °C. *J. Am. Chem. Soc.* **1999**, *121*, 5593–5594. [[CrossRef](#)]
68. Tomono, K.; Tsunobuchi, Y.; Nakabayashi, K.; Ohkoshi, S. Vanadium(II) Heptacyanomolybdate(III)-Based Magnet Exhibiting a High Curie Temperature of 110 K. *Inorg. Chem.* **2010**, *49*, 1298–1300. [[CrossRef](#)] [[PubMed](#)]
69. Mironov, V.S.; Bazhenova, T.A.; Manakin, Y.V.; Lyssenko, K.A.; Talantsev, A.D.; Yagubskii, E.B. A new Mo(IV) complex with the pentadentate (N3O2) Schiff-base ligand: the first non-cyanide pentagonal–bipyramidal paramagnetic 4d complex. *Dalton Trans.* **2017**, *46*, 14083–14087. [[CrossRef](#)] [[PubMed](#)]

